New Tungsten(VI) Guanidinato Complexes: Synthesis, Characterization, and Application in Metal−Organic Chemical Vapor Deposition of Tungsten Nitride Thin Films

Daniel Rische, Harish Parala, Eliza Gemel, Manuela Winter, and Roland A. Fischer*

Lehrstuhl für Anorganische Chemie II—Organometallics and Materials, Ruhr-Universität Bochum, Universitätsstrasse 150, D-44801 Bochum, Germany

Received August 24, 2006. Revised Manuscript Received October 11, 2006

Two new tungsten complexes, $[W(NtBu)_2(NMe_2)\{(iPrN)_2CNMe_2\}]$ (**2**) and $[W(NtBu)_2(H)\{(iPrN)_2CNMe_2\}]$ (**3**), as precursors for metal−organic chemical vapor deposition (MOCVD) of tungsten nitride thin films were synthesized from the starting compound $[W(NtBu)_2(Cl)\{(iPrN)_2CNMe_2\}]$ (**1**) by substitution of the chloro ligand by a dimethylamido and a hydrido group, respectively. Compounds **1**−**3** were characterized by ^{1}H NMR, ^{13}C NMR, EI-MS, IR, and elemental analysis including single-crystal X-ray diffraction studies on **1** and **3**. The thermal properties of the compounds were studied by thermogravimetric and differential thermal analysis. Precursors **2** and **3** were compared for the growth of tungsten nitride thin films by MOCVD. The obtained films were characterized by X-ray diffraction and scanning electron microscopy and by depth-profiling the composition with secondary neutron mass spectroscopy. Films grown without ammonia had surprisingly low nitrogen levels, indicating that **2** and **3** are not suited as single-source precursors for pure WN_x phases. When ammonia was used as a co reactant gas, the carbon content in the films decreased significantly and crystalline β-W_2N was obtained. Interestingly, films grown in the presence of ammonia by amido compound **2** yielded lower carbon contents than films obtained from hydrido compound **3**.

Introduction

Guanidinato ligands have recently attracted interest as nitrogen-rich, chelating ligands with high steric and electronic tunability. First reported by Lappert et al.,[1] they have been found to support main group metals[2−4] and transition metals[2,5−9] as well as lanthanides.[2,10] Due to their excellent steric and electronic tunability, guanidinato ligands have gained considerable attention beyond fundamental structural coordination chemistry. Guanidinato complexes proved to be excellent catalysts or initiators for various polymerization reactions.[11−15] Thus, guanidinato complexes appear to be quite promising as novel types of tailored homogeneous catalysts for a variety of reactions.

Even more recently, guanidinato complexes of aluminum and gallium[3] and of several early transition metals[5−7] have been found to be volatile (i.e., sublimable without decomposition), and so are suggested or have already been tested as metal−organic chemical vapor deposition (MOCVD) precursors. Nitrides of early transition metals play an important role in the miniaturization of micro electronic devices such as thin film capacitors or field effect transistors.[6−8,16] The international semiconductor road map includes the replacement of aluminum as an interconnect material by copper, due to its lower resistivity as a consequence of further miniaturization. However, copper easily diffuses into silicon and silicon dioxide, leading to destruction of the interconnections. Thus, stable diffusion barriers are required to ensure an appropriate lifetime of the device. Promising materials for this purpose are electrically conductive refractory nitrides and carbides of early transition metals such as TiN,[6] TaN,[7] HfN,[17] TiC_x,[18] WC_x,[19] or WN_x.[20−25] Tungsten nitride phases are particularly promising candidates.

* To whom correspondence should be addressed. E-mail: Roland.Fischer@rub.de.

(1) Chandra, G.; Jenkins, A. D.; Lappert, M. F.; Srivastava, R. C. *J. Chem. Soc. A* **1970**, 2550.
(2) Bailey, P. J.; Pace, S. *Coord. Chem. Rev.* **2001**, *214*, 91.
(3) Kenney, A. P.; Yap, G. P. A.; Richeson, D. S.; Barry, S. T. *Inorg. Chem.* **2005**, *44*, 2926.
(4) Chang, C.-C.; Hsiung, C.-S.; Su, H. L.; Srinivas, B.; Chiang, M. Y.; Lee, G.-L.; Wang, Y. *Organometallics* **1998**, *17*, 1585.
(5) Rische, D.; Baunemann, A.; Winter, M.; Fischer, R. A. *Inorg. Chem.* **2006**, *45*, 269.
(6) Carmalt, C. J.; Newport, A. C.; O'Neill, S. A.; Parkin, I. P.; White, A. J. P.; Williams, D. J. *Inorg. Chem.* **2005**, *44*, 615.
(7) Baunemann, A.; Rische, D.; Milanov, A.; Gemel, C.; Fischer, R. A. *Dalton Trans.* **2005**, 3051.
(8) Ong, T.-G.; Yap, G. P. A.; Richeson, D. S. *Chem. Commun.* **2003**, 2612.
(9) Zuckermann, R. L.; Bergman, R. G. *Organometallics* **2000**, *19*, 4795.
(10) Zhou, Y.; Yap, G. P. A.; Richeson, D. S. *Organometallics* **1998**, *17*, 4387.
(11) Zhou, L.; Sun, H.; Chen, J. Yao, Y.; Shen, Q. *J. Polym. Sci., Part A: Polym. Chem.* **2005**, *43*, 1778.
(12) Coles, M. P.; Hitchcock, P. B. *Eur. J. Inorg. Chem.* **2004**, 2662.
(13) Duncan, A. P.; Mullins, S. M.; Arnold, J.; Bergman, R. G. *Organometallics* **2001**, *20*, 1808.
(14) Bazinet, P.; Wood, D.; Yap, G. P. A.; Richeson, D. S. *Inorg. Chem.* **2003**, *42*, 6225.
(15) Luo, Y.; Yao, Y.; Shen, Q. *Macromolecules* **2002**, *35*, 8670.
(16) Nicolet, M. A.; Bartur, M. *J. Vac. Sci. Technol.* **1981**, *19*, 786.
(17) Kim, Y.; Baunemann, A.; Parala, H.; Devi, A.; Fischer, R. A. *Chem. Vap. Deposition* **2005**, *11* (6−7), 294.
(18) Wang, S. J.; Tsai, H. Y.; Sun, S. C. *J. Electrochem. Soc.* **2001**, *148* (8), C563.
(19) Kim, D.-H.; Kim, Y. J.; Song, Y. S.; Lee, B.-T.; Kim, J. H.; Suh, S.; Gordon, R. *J. Electrochem. Soc.* **2003**, *150* (10), C740.
(20) Crane, E. L.; Chiu, H.-T.; Nuzzo, R. G. *J. Phys. Chem. B* **2001**, *105*, 3549.

10.1021/cm061999d CCC: $33.50
Published on Web 11/15/2006

Scheme 1. Known Metal−Organic Tungsten Precursors

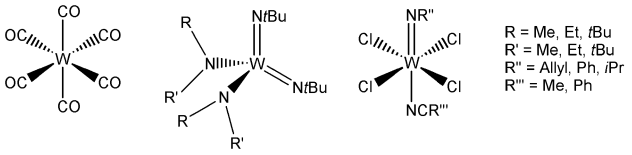

The method of choice of WN_x thin film deposition in microelectronics would be CVD or CVD-related techniques, if suitable precursors and processes were developed. In tungsten nitride CVD process, WF_6 is often used as a precursor,[26−30] having the disadvantage of corrosive HF as a reaction byproduct that might etch the silicon substrate, and of possible fluorine contamination of the films. Only a few halide-free metal organic compounds, suitable as MOCVD for WN_x materials precursors, are known to date (Scheme 1). Kelsey et al. obtained tungsten nitride from tungsten hexacarbonyl and ammonia.[31] A precursor type suitable for liquid injection CVD is the monoimido tetrachloro complexes reported by Bchir et al.[24,25] Another type of precursor is the bis(*tert*-butylimido) dialkylamido complexes, first synthesized by Nugent and Harlow.[32] This latter class of precursors is used not only in MOCVD of tungsten nitride,[20,21] but also in atomic layer deposition (ALD) of tungsten nitride[22,23] and of tungsten carbide.[18] Quite recently, some tungsten guanidinates have been suggested as liquid injection CVD precursors.[33] We have also successfully demonstrated the use of guanidinato ligands to obtain tailored MOCVD single-source precursors for metal nitrides, in particular focusing on TaN.[7] In addition, we have started to transfer this knowledge to the precursor chemistry of WN_x materials and have reported on the synthesis and structural chemistry of mixed guanidinato/alkylimido/azidotungsten(VI) complexes.[5] However, investigation of the thermal properties of these previously reported tungsten compounds yielded unsatisfactory results, and these compounds are not volatile enough to use for MOCVD processes. In an attempt to fine-tune the precursor properties by varying the ligand combinations, we were able to synthesize two new volatile tungsten complexes with

Scheme 2. Synthesis of the New Tungsten Precursors

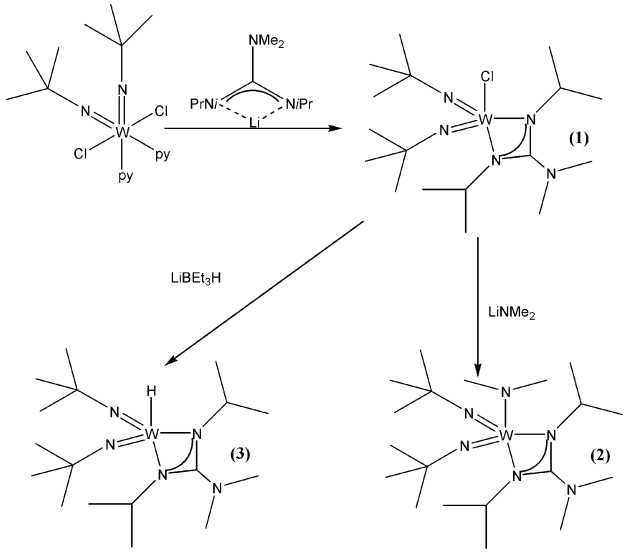

improved thermal properties. Now herein, we report on the synthesis, structure, and MOCVD application of two new tungsten guanidinato complexes, $[W(NtBu)_2(NMe_2)\{(iPrN)_2CNMe_2\}]$ (**2**) and $[W(NtBu)_2(H)\{(iPrN)_2CNMe_2\}]$ (**3**), which we derived from the known starting compound $[W(NtBu)_2Cl_2py_2]$ (Scheme 2).[5,22] The two compounds exhibit an identical set of ligands, except the dimethylamido group of compound **2** is replaced by a hydrido ligand in compound **3**. The two closely related tungsten compounds were tested and compared in MOCVD processes for the growth of tungsten nitride thin films with ammonia and without ammonia as an additional reactant gas. The basic properties of thin films of WN_x were characterized in some detail.

Experimental Section

A. General Procedures. All manipulations were performed in an inert atmosphere (Ar) glovebox or using standard Schlenck techniques. All reaction solvents were purified using an automatic solvent purification system (MBraun) directly connected to a glove box ($[H_2O] < 1$ ppm, Karl Fischer), except CH_2Cl_2, which was used in p.a. quality without further purification. $[W(NtBu)_2Cl_2py_2]$ (py = pyridine) was prepared by a literature procedure.[5] *N*,*N*′-Diisopropylcarbodiimide (98% purity) and lithium triethylboron hydride (1 mol/L in THF) were purchased from Acros, and lithium dimethylamide (95% purity) was purchased from Aldrich.

The single-crystal X-ray diffraction measurements of compounds **1** and **3** were performed on an Oxford Excalibur-2 diffractometer. All structures were solved by direct methods (SHELXL-97) and refined by a full-matrix least-squares method based on F^2 using SHELXL-97. The files CCDC-615607 (**1**) and CCDC-615608 (**3**) contain the supplementary crystallographic data for this structure. These data can be obtained free of charge via http://www.ccdc.cam.ac.uk/conts/retrieving.html. See also Table 1.

NMR spectra were measured on a Bruker Avance DPX 250 spectrometer. All spectra were recorded at 25 °C. Deuterated benzene (99.5% purity) was purchased from Deutero GMBH and was degassed and dried over activated molecular sieves (4 Å). Mass spectra were recorded, using a Varian MAT spectrometer. IR spectra were measured on a Perkin-Elmer 1720 X.

Thermogravimetric and differential thermal analysis (TG/DTA) was carried out using a Seiko TG/TDA 6300S11 instrument (sample size ∼10 mg), with a heating rate of 5 °C/min. All measurements

(21) (a) Wu, J.-B.; Yang, Y.-W.; Lin, Y.-F.; Chiu, H.-T. *J. Vac. Sci. Technol., A* **2003**, *21* (5), 1620. (b) Dezelah, C. L., IV; El-Kadri, O. M.; Szilágyi, I. M.; Campbell, J. M.; Arstila, K.; Niinistö, L.; Winter, C. H. *J. Am. Chem. Soc.* **2006**, *128*, 9638.
(22) Becker, J. S.; Suh, S.; Wang, S.; Gordon, R. *Chem. Mater.* **2003,** *15*, 2969.
(23) Becker, J. S.; Gordon, R. *Appl. Phys. Lett.* **2003**, *82* (14), 2239.
(24) Bchir, O. J.; Green, K. M.; Ajmera, H. M.; Zapp, E. A.; Anderson, T. J.; Brooks, B. C.; Reitford, L. L.; Powell, D. H.; Abboud, K. A.; McElwee-White, L. *J. Am. Chem. Soc.* **2005**, *127*, 7825.
(25) Bchir, O. J.; Green, K. M.; Anderson, T. J.; Brooks, B. C.; McElwee-White, L. *J. Cryst. Growth* **2004**, *261*, 280.
(26) Kim, S.-H.; Oh, S. S.; Kim, K.-B.; Kang, D.-H.; Li, W.-M.; Haukka, S.; Touminen, M. *Appl. Phys. Lett.* **2003**, *82* (25), 4486.
(27) Kim, S.-H.; Oh, S. S.; Kim, H.-M.; Kang, D.-H.; Kim, K.-B.; Li, W.-M.; Haukka, S.; Touminen, M. *J. Electrochem. Soc.* **2004**, *151* (4), C272.
(28) Klaus, J. W.; Ferro, S. J.; George; S. M. *Appl. Surf. Sci.* **2000**, *162*−*163*, 479.
(29) Ganguli, S.; Chen, L.; Levine, T.; Zheng, B.; Chang, M. *J. Vac. Sci. Technol., B* **2000**, *18* (1), 237.
(30) Hoyas, A. M.; Schuhmacher, J.; Shamiryan, D.; Waeterloos, J.; Besling, W.; Celis, J. P.; Maex, K. *J. Appl. Phys.* **2004**, *95* (1), 381.
(31) Kelsey, J. E.; Goldberg, C.; Nuesca, G.; Peterson, G.; Kaloyeros, A. E.; Arkles, B. *J. Vac. Sci. Technol., B* **1999**, *17* (3), 1101.
(32) Nugent, W. A.; Harlow, R. L. *Inorg. Chem.* **1980**, *19*, 777.
(33) Wilder, C. B.; Reitford, L. L.; Abboud, K. A.; McElwee-White, L. *Inorg. Chem.* **2006**, *45*, 263.

Table 1. Crystallographic Data for Compounds 1 and 3

	1	**3**
empirical formula	$WClN_5C_{17}H_{38}$	$WCl_2N_5C_{18}H_{41}$
fw	531.824	582.31
space group	*C*2/*c*	$P2_1/n$
a (Å)	15.399(2)	8.8327(6)
b (Å)	9.5815(15)	19.0411(13)
c (Å)	32.617(5)	15.2788(10)
α (deg)	90	90
β (deg)	103.140(15)	101.430(6)
γ (deg)	90	90
V (Å^3)	4686.5(12)	2518.7(3)
Z	1	4
ρ_{calcd} (g cm^{-3})	1.507	1.536
μ (mm^{-1})	5.052	4.810
R1	0.0528	0.0263
wR2	0.0863	0.0415

were performed under atmospheric pressure in the temperature range of 25−500 °C under a flowing high-purity (99.9999%) nitrogen atmosphere.

B. Synthesis of the Tungsten Nitride Precursors. *[W(NtBu)$_2$(Cl){(iPrN)$_2$CNMe$_2$}] (**1**).* A 0.55 g portion of $LiNMe_2$ (10.8 mmol) was suspended in 60 mL of hexane. A 1.67 mL portion of *N*,*N*′-diisopropylcarbodiimide (10.8 mmol) was added, and the mixture was stirred until a clear solution formed. This solution was transferred to another solution of 6 g of $[W(NtBu)_2Cl_2py_2]$ (10.8 mmol) dissolved in 60 mL of toluene. The reaction mixture was allowed to stir overnight. The solution was filtered, and the solvent was stripped to leave a yellow crude product, which was recrystallized from toluene to yield 4.6 g of pale yellow crystals (80%). ^{1}H NMR (250 MHz, C_6D_6): *δ* 1.09 (d, 6H, N*i*Pr); 1.51 (s, 18H, N*t*Bu); 1.57 (d, 6H, N*i*Pr); 2.19 (s, 6H, NMe_2); 3.79 (sept, 1H, N*i*Pr); 3.91 (sept, 1H, N*i*Pr). ^{13}C NMR (250 MHz, C_6D_6): *δ* 23.7 (*Me*$_2$CHN); 24.5 (*Me*$_2$CHN); 32.6 (NC*Me*$_3$); 39.4 (*Me*$_2$N); 45.7 (Me$_2$*C*HN); 48.8 (Me$_2$*C*HN); 67.5 (N*C*Me$_3$); 168.4 (*C*N$_3$). EI-MS [*m*/*z* (relative intensity, %)]: 531 (2) [M$^+$]; 516 (1) [M$^+$ − Me]; 390 (9) [M$^+$ − 2N*t*Bu]; 71 (18) [N*t*Bu]; 58 (100) [*t*BuH]; 44 (22) [NMe_2]; 29 (10) [HCN]. Anal. Calcd for $WClN_5C_{17}H_{38}$: C, 38.39; H, 7.20; N, 13.17. Found: C, 38.69; H, 7.29; N, 12.59.

*[W(NtBu)$_2$(NMe$_2$){(iPrN)$_2$CNMe$_2$}] (**2**).* A 0.2 g portion of $LiNMe_2$ (3.8 mmol) was suspended in 30 mL of hexane. A solution of 2 g of **1** (3.8 mmol) in toluene was added, and the whole mixture was allowed to stir overnight. The reaction mixture was filtered, and the solvent was stripped off, leaving a yellow solid crude product which was sublimed at 100 °C and 10^{-3} mbar to yield 1.4 g (68%) of a yellow solid. ^{1}H NMR (250 MHz, C_6D_6): *δ* 1.27 (d, 12H, N*i*Pr); 1.51 (s, 18H, N*t*Bu); 2.36 (s, 6H, NMe_2); 3.55 (s, 6H, NMe_2); 3.83 (sept, 2H, N*i*Pr). ^{13}C NMR (250 MHz, C_6D_6): *δ* 24.4 (*Me*$_2$CHN); 32.6 (*Me*$_2$CHN); 34.3 (NC*Me*$_3$); 39.9(Me$_2$*C*HN) 46.5 (Me$_2$*C*HN); 55.8 (*Me*$_2$N); 66.7 (N*C*Me$_3$); *C*N$_3$ not detectable. EI-MS [*m*/*z* (relative intensity, %)]: 540 (12) [M$^+$]; 495 (100) [M$^+$ − NMe_2 − H]; 482 (7) [M$^+$ − *t*Bu]; 454 (10) [M$^+$ − 2*i*Pr]; 438 (4) [M$^+$ − 2*i*Pr − Me − H]; 413 (6) [M$^+$ − (*i*PrN)$_2$C]; 399 (34) [M$^+$ − 2*t*Bu]; 273 (11) [W(NMe$_2$)$_2$)]; 171 (5) [H(*i*PrN)$_2$CNMe$_2$]; 114 (11) [*i*PrNHCNMe$_2$]; 99 (12) [*i*PrNCN$_2$H$_2$]; 85 (9) [*i*PrNCNH$_2$]; 71 (19) [N*t*Bu]; 58 (26) [H*t*Bu]; 43 (18) [*i*Pr]; 29 (6) [HCN]. Anal. Calcd for $WN_6C_{19}H_{44}$: C, 42.23; H, 8.21; N, 15.55. Found: C, 42.14; H, 8.12; N, 15.13.

*[W(NtBu)$_2$(H){(iPrN)$_2$CNMe$_2$}] (**3**).* A 4.6 g portion of **1** (8.6 mmol) was dissolved in 40 mL of toluene, and 8.6 mL of $LiBEt_3H$ in THF (1 mol/L) was added. The solution was heated to 80 °C overnight. Now about a quarter of the solvent volume was stripped in a vacuum, and the resulting solution was filtered. The residual solvent was stripped to yield to brown crude product which was sublimed at 100 °C and 10^{-3} mbar to yield 2 g (47%) of a beige solid. Crystals suitable for X-ray crystallography were grown by cooling a saturated solution of **3** in methylene chloride. ^{1}H NMR (250 MHz, C_6D_6): *δ* 1.22 (d, 6H, N*i*Pr); 1.26 (d, 6H, N*i*Pr); 1.54 (s, 18H, N*t*Bu); 2.15 (s, 6H, NMe_2); 3.70 (sept, 2H, N*i*Pr); 12.59 (s, 1H, WH). ^{13}C NMR (250 MHz, C_6D_6): *δ* 26.8 (*Me*$_2$CHN); 27.8 (*Me*$_2$CHN); 37.2 (NC*Me*$_3$); 41.5 (*Me*$_2$N); 47.7 (Me$_2$*C*HN); 48.7 (Me$_2$*C*HN); 68.8 (N*C*Me$_3$); 172.8 (*C*N$_3$). FT-IR (KBr, cm^{-1}): 2967 s (ν_{C-H}); 1854 s (ν_{W-H}). EI-MS [*m*/*z* (relative intensity, %)]: 497 (43) [M$^+$]; 482 (13) [M$^+$ − Me]; 454 (12) [M$^+$ − *i*Pr]; 413 (5) [M$^+$ − *i*Pr − NMe_2 + H]; 370 (4) [(*t*BuN)$_2$WNMe_2]; 356 (12) [M$^+$ − 2*t*Bu]; 310 (4) [W(N*i*Pr)$_2$C]; 298 (4) [W(N*i*Pr)$_2$]; 282 (4) [WHN*i*PrCN_2]; 255 (7) [WN*t*Bu]; 171 (8) [H(N*i*Pr)$_2$CNMe_2]; 156 (4) [H(N*i*Pr)$_2$CNMe]; 113 (11) [*i*PrNCNMe_2]; 99 (13) [*i*PrNC(NH)$_2$]; 85 (9) [Me$_2$NCN_2H]; 71 (53) [N*t*Bu]; 58 (100) [*t*BuH]; 41 (30) [CH_3CHCH_2]; 29 (9) [HCN]. Anal. Calcd for $WN_5C_{17}H_{39}$: C, 41.05; H, 7.90; N, 14.08. Found: C, 40.78; H, 8.53; N, 13.99.

C. MOCVD of Tungsten Nitride. All thin film depositions were carried out in a home-built horizontal cold wall, glass reactor described elsewhere.[17] The thin film depositions were carried out on Si(100) substrates using N_2 (99.9999%) as a carrier gas. NH_3 (99.995%) was used as a reactive gas wherever indicated. Prior to the MOCVD experiments, the substrates were cleaned using a standard method and the native oxide layer was not removed (treated with ultrasound and subsequently washed and cleaned with 2-propanol and acetone). The substrates were placed on a Si_3N_4 susceptor which was resistively heated to the desired temperature. A U-shaped glass tube with Teflon stoppers on both sides, a connection for the carrier gas on one side, and a connection to the reactor on the other side was used as an evaporator. The bubbler and the delivery lines were heated by heating tapes set at 100 °C for the delivery lines. A bubbler temperature of 100 °C was used for compound **2**. Compound **3** was heated to 90 °C. The reactor had a base pressure of 10^{-5} mbar. All depositions were carried out at 1 mbar of pressure and a carrier gas (N_2) flow rate of 20 sccm. When NH_3 was used as a co reactant gas, a flow rate of 25 sccm was used. The deposition time was set to 60 min for all MOCVD experiments.

D. Film Characterization. X-ray diffraction (XRD) measurements were performed using a Bruker AXS D8-Advance diffractometer with Cu Kα radiation to investigate the crystallinity of the films. The composition of the films was determined by depth-profiling using SNMS (secondary neutral mass spectroscopy) measurements employing a VG SIMSLABB IIIA instrument [MATS (UK) Ltd.]. The primary ion beam was argon at 10 keV, usually operated at high currents (0.8−1.0 *μ*A) over large areas (0.5 to 4 mm raster size) depending on the total depth requirements. The surface morphology and thickness measurements of the films were determined by scanning electron microscopy (SEM) (LEO (Zeiss) 1530 Gemini instrument), while resistivity measurements were conducted using a standard four-point probe unit (Jandel). The film thickness and corresponding growth rates were estimated by cross-sectional SEM analysis.

Results and Discussion

A. Precursor Synthesis and Spectroscopic and Structural Characterization. Reaction of $[W(NtBu)_2Cl_2py_2]$ with 1 equiv of the in situ formed Li(N*i*Pr)$_2$CNMe_2 and recrystallization from toluene yielded compound **1** as pale yellow crystals (Scheme 1). The proton NMR displays one singlet for the *tert*-butylimido group at 1.51 ppm and one at 2.19 ppm for two methyl groups at the guanidinato ligand. It also reveals two doublets (1.09 and 1.57 ppm) and two septets (3.79 and 3.91 ppm) belonging to two chemically different isopropyl groups. The EI-MS of **1** shows the expected molecular ion peak [M$^+$] at *m*/*z* = 531 (2% relative intensity)

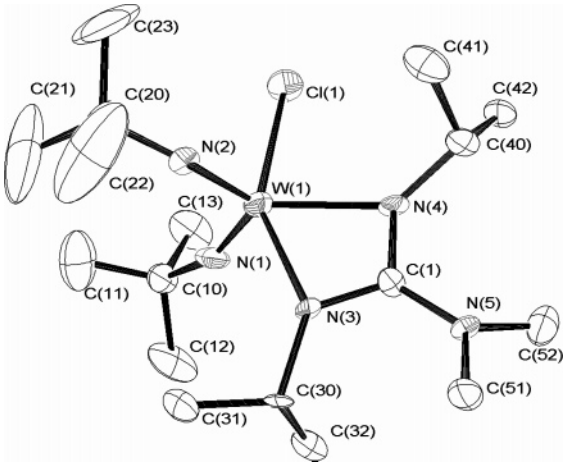

Figure 1. Molecular structure of compound **1** in the solid state (ellipsoid probability 50%). Selected bond lengths (Å) and angles (deg): W(1)−N(1), 1.753(7); W(1)−N(2), 1.693(7); W(1)−N(3), 2.125(6); W(1)−N(4), 2.169-(7); W(1)−Cl(1), 2.385(2); N(1)−W(1)−N(2), 112.1(3); N(1)−W(1)−N(3), 99.9(3); N(1)−W(1)−N(4), 125.3(3); N(1)−W(1)−Cl(1), 96.7(2); N(2)−W(1)−N(3), 101.3(3); N(2)−W(1)−N(4), 121.6(3); N(2)−W(1)−Cl(1), 97.5(2); N(3)−W(1)−N(4), 61.6(2); N(3)−W(1)−Cl(1), 148.01(17); N(4)−W(1)−Cl(1), 86.54(17).

and another peak of similar intensity at $m/z = 516$ that was assigned to the loss of one methyl group [$M^+ - CH_3$]. The peak at $m/z = 390$ (9% relative intensity) was attributed to a fragment ion containing the guanidinato ligand and the remaining chloro ligand bonded to the tungsten center [$M^+ - 2N$*t*Bu].

The molecular structure of compound **1** in the solid state derived from single-crystal X-ray diffraction studies is shown in Figure 1. The strongly distorted trigonal bipyramidal coordination mode at the tungsten center is expectedly quite similar to that of the closely related congener [W(N*t*Bu)$_2$(Cl){[(N*i*Pr)$_2$CN*i*Pr$_2$}],[5] which we have reported earlier; the N atoms of the imido groups and one N atom of the guanidinato ligand form the equatorial plane with a sum of angles of 359°, while the chloro ligand occupies an axial position. The same is true for **1** with a sum of angles in the CN_3 plane of 359.9°. The second N atom of the guanidinato ligand is shifted out of the ideal axial position due to its linkage to the rest of the ligand. Nevertheless, the sum of angles in the Cl(1)−N(3)−N(4) plane around the tungsten is 360.13°, as expected for a trigonal bipyramidal coordination geometry.

The treatment of **1** with 1 equiv of lithium dimethylamide yields compound **2** as a yellow powder. The proton NMR shows the singlets for the dimethylamido group, the methyl groups at the guanidinate, and the imido groups. Similar to [W(N*t*Bu)$_2$(NMe$_2$){(N*i*Pr)$_2$CN*i*Pr$_2$}],[5] the two isopropyl groups have equivalent NMR shifts, which points to a more symmetrical environment of the guanidinato ligand, which can be explained by the higher steric demand of the dimethylamido group compared to that of a chloro ligand, forcing the complex into a more symmetrical structure with equivalent environments for the *i*PrN groups coordinated to the tungsten center. In addition, the higher π-donor ability of the amido group with respect to the chloro ligand has to be taken into account too. However, more detailed computational analysis of the particular bonding situation is beyond the scope of this work here. The EI-MS of **2** reveals the molecular peak at $m/z = 540$ (12% relative intensity). The peak at $m/z = 495$ (100% relative intensity) is assigned to the cleavage of a dimethylamido group, the peak at $m/z = 482$ (7% relative intensity) is attributed to the loss of a *tert*-butyl group, and the peak at $m/z = 454$ (10% relative intensity) most likely relates to the loss of two isopropyl groups. Peaks with $m/z \leq 171$ can be assigned to fragmentation of the guanidinato ligand, except the peak at $m/z = 58$ (26% relative intensity), which may have its origin in fragmentation of the guanidinato ligand as well as from the *t*Bu residue at the imido ligand. Unfortunately, we were not able to grow single crystals of **2** suitable for X-ray diffraction studies to unambiguously clarify the molecular structure of **2** in the solid state.

Adding 1 equiv of LiBEt$_3$H solution to compound **1** and heating it overnight yields the hydrido compound **3**. The proton NMR shows the signal of the hydrido ligand at 12.59 ppm, which could be identified by its tungsten satellites, revealing a coupling constant of $^1J_{W-H} = 96.8$ Hz. This is an unusual downfield shift of a hydrido ligand, with a few examples in the literature.[34−36] According to the smaller steric bulk of the hydrido ligand, the NMR exhibits two different signals for the N*i*Pr groups, like described above for **1** but with a smaller splitting of the signals. Hydrogen gas evolution occurs when **3** is dissolved in methanol, which indicates the hydridic character of the W−H bond. The EI-MS nicely displays the molecular peak at $m/z = 497$ (43% relative intensity). The fragmentation pattern of **3** is very similar to that of **2**, referring to the nearly identical set of ligands of the two complexes. The IR spectrum exhibits an absorption band at 1854 cm^{-1}, which is a typical value for W−H stretching frequencies.[34,37]

The molecular structure of **3** in the solid state as obtained from single-crystal X-ray diffraction studies is shown in Figure 2. One solvent molecule per complex has been included in the elementary cell. The hydrido ligand could not be located in the difference Fourier maps but was included in the structure refinement in a typical position and then refined. Compound **3** adopts a trigonal bipyramidal coordination geometry quite similar to that of **1**, with the estimated position of the hydrido group at the axial place and the imido ligands and the N(4) atom forming the equatorial plane, where the sum of angles around the tungsten is 359.9°.

B. Thermal Characterization of Compounds 2 and 3. Simultaneous TG/DTA was carried out to investigate the suitability of the compounds for CVD application (Figure 3). Compounds **2** and **3** are low melting point solids (62 and 73 °C) which begin to volatilize at about 105 °C (under ambient pressure). For both compounds the onsets of volatilization (∼105 °C) fall in the same temperature range, but the temperature ranges of decomposition are quite

(34) Holmes, S. M.; Schafer, D. F., II; Wolczanski, P. T.; Lobkovsky, E. B. *J. Am. Chem. Soc.* **2001**, *123*, 10571.
(35) Schrock, R. R.; Shih, K.-Y.; Dobbs, D. A.; Davis, W. M. *J. Am. Chem. Soc.* **1995**, *117*, 6609.
(36) Chisholm, M.; Eichhorn, B. W.; Huffman, J. C. *Organometallics* **1989**, *8*, 67
(37) van der Zeijden, A. A. H.; Sontag, C.; Bosch, H. W.; Shklover,V.; Berke, H. *Helv. Chim. Acta* **1991**, *74*, 1194.

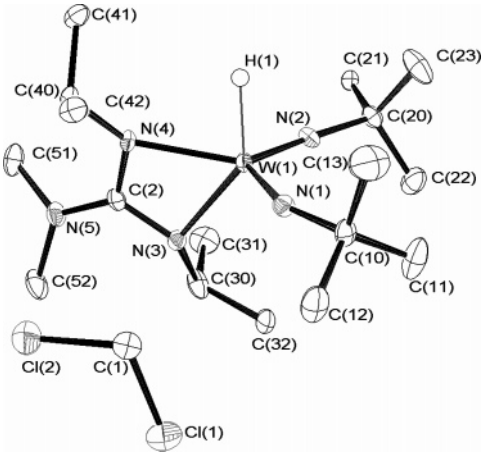

Figure 2. Molecular structure of compound **3** as a methylene chloride solvate in the solid state (ellipsoid probability 50%). Selected bond lengths (Å) and angles (deg): W(1)−N(1), 1.758(2); W(1)−N(2), 1.752(2); W(1)−N(3), 2.149(2); W(1)−N(4), 2.1603(19); N(1)−W(1)−N(2), 112.83(9); N(1)−W(1)−N(3), 107.28(9); N(1)−W(1)−N(4), 121.88(9); N(2)−W(1)−N(3), 106.97(9); N(2)−W(1)−N(4), 125.19(9); N(3)−W(1)−N(4), 60.77(8).

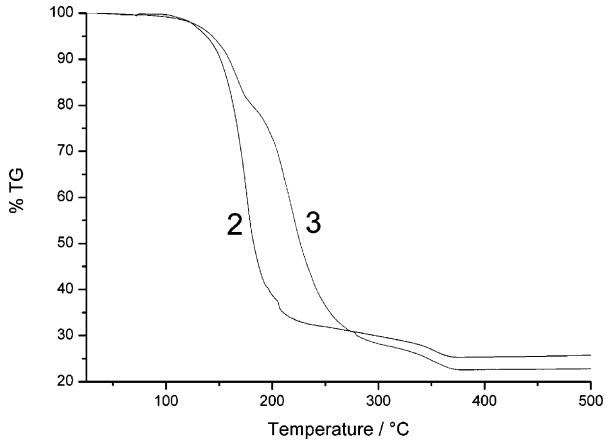

Figure 3. TG analysis of compounds **2** and **3** at a heating rate of 5 °C/min.

different. In the case of compound **2**, the TG curve shows almost a single-step decomposition behavior, while the TG curve of compound **3** clearly reveals a multistep decomposition pattern. It can be seen that the volatilization of compound **2** starts at 105 °C with a rather constant evaporation up to 205 °C. An inflection point corresponding to the onset of a decomposition process can be seen around 205 °C. A second inflection point is observed around 370 °C, and the weight loss remains almost constant at higher temperatures. In the case of compound **3** the TG curve shows a constant weight loss up to 175 °C. Evaluation of the TG plot shows two shoulder curves corresponding to multistep decomposition behavior of compound **3** (from 175 to 275 °C and from 275 to 370 °C). In both the cases, there is a sufficient temperature window between sublimation and decomposition, which renders these compounds suitable for MOCVD application. Residual masses of 25% and 22% were observed for compounds **2** and **3**, respectively, in TG analyses, which are lower than the residual masses expected for the most likely W_2N phase (38% and 35%).

C. MOCVD Experiments. To evaluate the suitability of compounds **2** and **3** in thin film deposition application, several preliminary control MOCVD experiments were carried out with and without NH_3. All experiments were carried out in the temperature range of 400−800 °C. All obtained films were shiny with a mirror-like appearance. Films deposited below 500 °C were amorphous without X-ray diffraction features, while those deposited at and above 500 °C were polycrystalline. The obtained films were characterized by XRD, SEM, cross-sectional SEM, SNMS depth-profiling analysis, and resistivity measurements.

Figure 4 shows the effect of the deposition temperature on the thin film crystallinity using compound **2** *without* ammonia. When the deposition temperature was increased from below 500 to 600−800 °C, the deposited material started to exhibit crystalline domains as indicated in the XRD; two broad peaks around $2\theta = 37.73°$ and 43.84° were observed, corresponding to cubic β-W_2N and the (111) and (200) lattice planes. The parallel formation of ternary β-WN_xC_y or binary β-WC (or related phases) cannot be ruled out from the XRD analysis, as the observed peaks are too broad and the (111) peak positions of the binary β-W_2N and β-W_2C phases are very close to each other with 2θ values of 37.74° and 36.98°, respectively. The additional peak at 33.03° represents Si(200) Kα radiation. No other detectable peaks corresponding to metallic tungsten or tungsten oxide phases were observed. When additional NH_3 was used as a reactive gas during the depositions, even at 500 °C a sharpening of the X-ray diffraction peaks was observed (Figure 4b). Clearly the presence of ammonia is beneficial for the growth of larger crystalline domains (grains). This effect increases with increasing temperature possibly due to the insufficient surface diffusion of NH_3 or NH_x dissociated species at lower deposition temperatures.

SEM analysis (Figure 5a) of films grown from precursor **2** without NH_3 indicates a smooth surface with uniform distribution of small grains having similar shapes and dimensions. The inset figure shows the cross-sectional SEM image. The image indicates the existence of columnar-type growth of the grains. The SEM micrograph of the films deposited with NH_3 using compound **2** (Figure 5b) shows a different surface morphology with almost uniform grain size and shape, as well as an increase of the average grain size (∼350 nm) as anticipated from the XRD data. These larger crystals, i.e., elongated cone-shaped grains, are well conglomerated and uniformly distributed throughout the substrate surface. Again, cross-sectional SEM substantiates the columnar growth mode (Figure 5b).

SNMS depth-profiling was used to determine the film composition throughout the layer down to the interface to the substrate. Without ammonia, both precursors yielded films with high carbon contents (50−60%) and surprisingly low nitrogen levels (<5%), which is consistent with previously reported results of Kim et al.[19] and of Bchir et al.,[24] who used $W(NtBu)_2(NMe_2)_2$[19] and $Cl_4(RCN)W(NC_3H_5)$ (R = Me, Ph)[24] as precursors for tungsten nitride film growth, respectively. However, this finding is in sharp contrast to our related work on TaN MOCVD using similar guanidinato precursors, e.g., [Ta(NMeEt){η^2-(N*i*Pr)$_2$C(NMeEt)}(N*t*Bu)], which gave very pure, stoichiometric and carbon-free cubic TaN in the absence of ammonia![5,7] From the SNMS data (see the Supporting Information) one can infer that the films

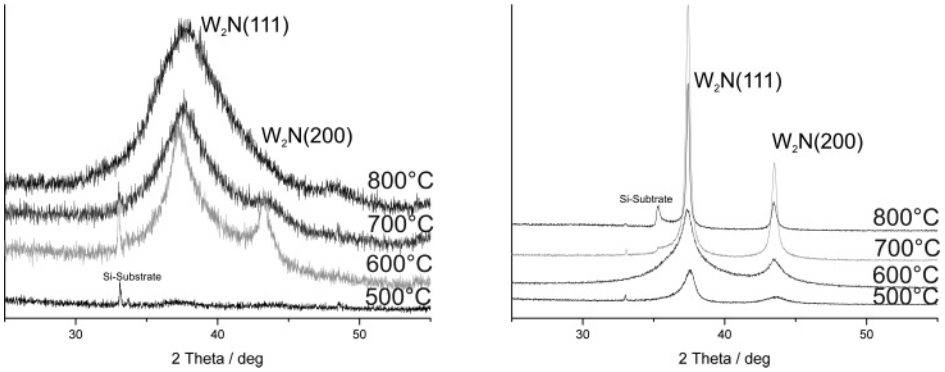

Figure 4. XRD of films deposited without NH_3 (a, left) and with NH_3 (b, right) using compound **2** at different deposition temperatures.

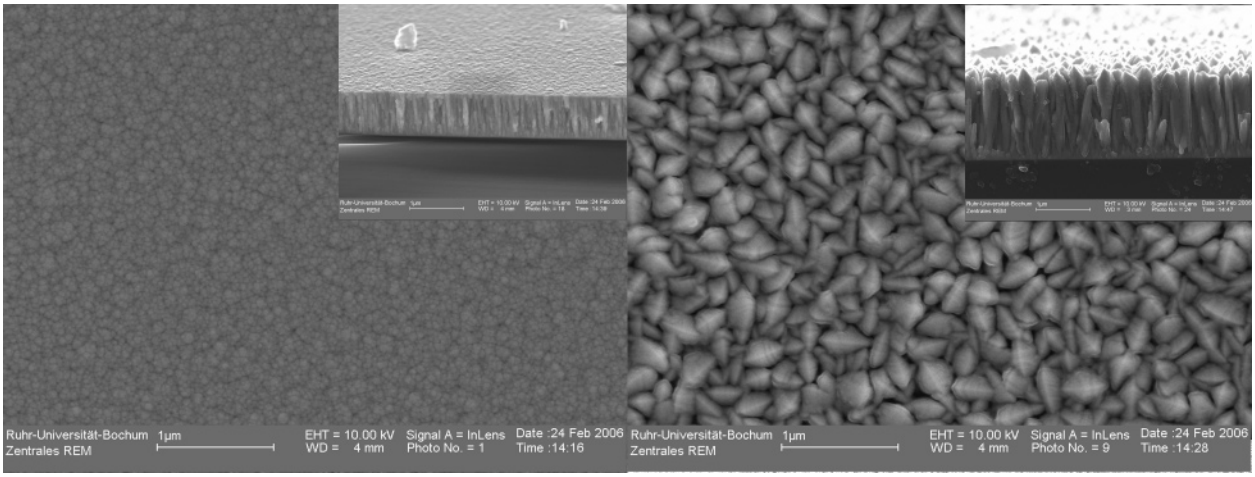

Figure 5. SEM and cross-sectional SEM images of films deposited without NH_3 (a, left) and with NH_3 (b, right) using compound **2** at 800 °C.

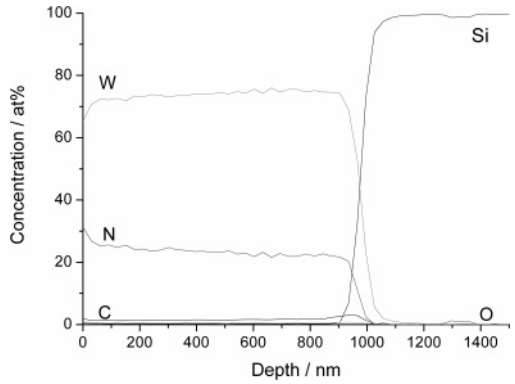

Figure 6. SNMS analysis of a film deposited with NH_3 using compound **2** at 800 °C.

are likely to contain the mixed phases of β-WN_xC_y as well as β-W_2N and β-WC. In addition, the presence of more or less of the amorphous tungsten oxynitride phase, $W(N,O)_x$, cannot be ruled out. When additional NH_3 was used as a co reactant gas during the depositions with precursor **2**, a nitrogen level of 23 atom % and a tungsten concentration of 73 atom % were obtained throughout the film thickness, pointing to the β-W_2N composition (Figure 6). As expected, addition of NH_3 dramatically increases the N concentration and decreases the C content in the film. This is probably due to the enhanced NH_3 decomposition at higher temperatures, which may favor the desorption of hydrocarbon-containing fragments from the surface and likely scavenging of the carbon species from the film. Another possibility could be that the ammonia is acting as a catalyst for the cleavage of the ligands, as reported by Becker et al. for $[W(NtBu)_2(NMe_2)_2]$.[22]

When compound **3** was used in MOCVD experiments, addition of NH_3 again proved favorable in terms of selective growth of the desired tungsten nitride phase. The crystallinity of the films (Figure 7a) increases drastically. SEM images (Figure 8) document growth morphology similar to that discussed in the case of compound **2**. SNMS depth-profiling (Figure 9) reveals that in contrast to compound **2** the addition of NH_3 causes an unexpected drop in the N level throughout the film with a surprisingly high carbon incorporation of 11 atom %. Nevertheless, the SNMS results indicate a substantial increase in N concentration for these films relative to those grown without NH_3, which is in consistent with the results obtained from compound **2**. The increase in the C concentration may be due to the prereaction of compound **3** with NH_3 (where NH_3 could act as a reducing agent at higher temperatures), resulting in precursor decomposition, prior to the thin film growth, which may increase the carbon content in the film. As observed in the TG analysis, compound **3** showed multistep decomposition behavior unlike in the case of compound **2**. Clearly, a more detailed investigation of the decomposition behaviors of compounds **2** and **3** is warranted and will be presented in a separate study elsewhere.

Growth rates of MOCVD experiments were calculated by dividing the film thickness (obtained from cross-sectional SEM analysis) by the deposition time. Compounds **2** and **3** showed similar trends with respect to the deposition rate without NH_3, and the growth rate was increased with an

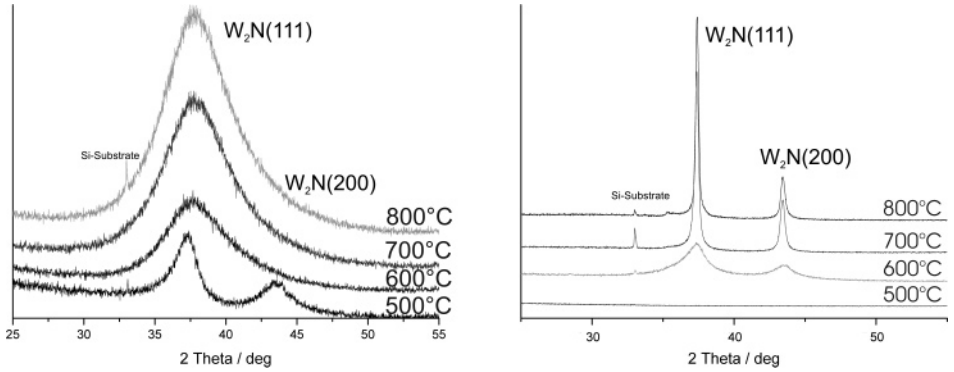

Figure 7. XRD of films deposited without NH_3 (a, left) and with NH_3 (b, right) using compound **3** at different deposition temperatures.

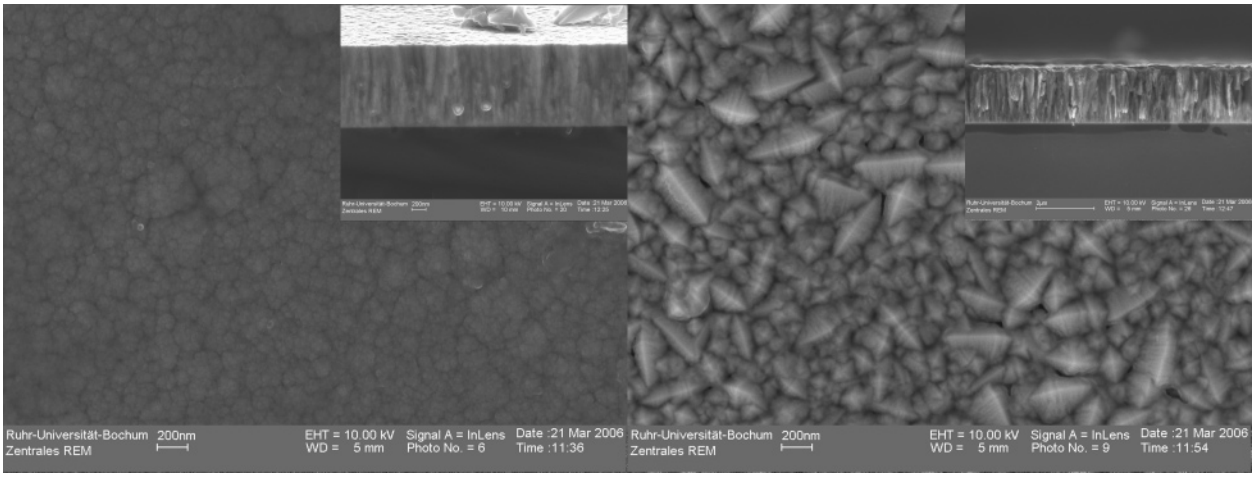

Figure 8. SEM and cross-sectional SEM images of films deposited without NH_3 (a, left) and with NH_3 (b, right) using compound **3** at 700 °C.

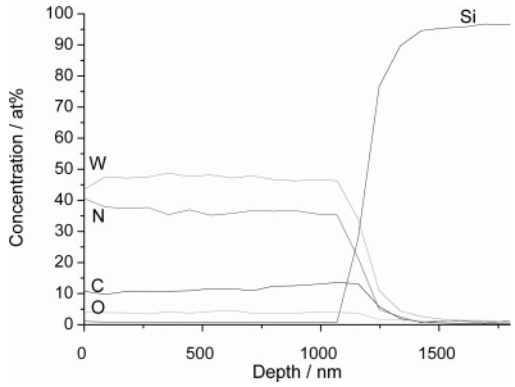

Figure 9. SNMS analysis of a film deposited with NH_3 using compound **3** at 700 °C.

increase in the deposition temperature (both cases). In the case of compound **2** the growth rate was increased from 2.8 nm/min (at 500 °C) to 13.6 nm/min (at 800 °C), and in the case of compound **3** the range of the growth rate increased from 6.3 to 19.1 nm/min. As expected, with both the compounds, the addition of NH_3 increases the growth rate with increasing deposition temperature, i.e., for compound **2** from 4.23 to 58.28 nm/min and for compound **3** from 3.0 to 32.4 nm/min. However, in the case of depositions without NH_3, compound **3** showed higher growth rates compared to compound **2**, while, in the case of depositions with NH_3, compound **2** had higher growth rates than compound **3**. Such an increase in the growth rate with NH_3 depositions with compound **2** may arise from the precursor decomposition pathways such as β-hydrogen elimination from the dimethylamido ligand of compound **2**. Resistivity measurements of the films deposited from both compounds **2** and **3** showed fairly good values for films deposited with and without NH_3. Films deposited from compound **2** at 500 °C (amorphous film) with NH_3 revealed the lowest resistivity value of 207 $\mu\Omega$·cm, and 660 $\mu\Omega$·cm was measured for the film deposited with compound **3** at 500 °C with NH_3. In the case of the depositions with NH_3 the film resistivity increases with the deposition temperature, and at 800 °C films grown from compounds **2** and **3** showed resistivity values of 1238 and 1337 $\mu\Omega$·cm, respectively. This is likely due to an increase in the nitrogen concentration in the film, which is known to increase the film resistivity. Similar observations are reported in the literature, where a resistivity decrease is expected with decreasing nitrogen content in WN_x films.[38,39] Adhesion of the films to the substrates was tested by the Scotch tape test. It was observed that films deposited at lower temperatures ($T \leq 600$ °C) had low adhesion to the substrate, while films deposited at high temperatures were impossible to remove from the substrate by this test.

Conclusion

Two new tungsten guanidinato complexes with identical ligand sets, except a dimethylamido ligand (compound **2**) and a hydrido ligand (compound **3**), have been synthesized and characterized in detail. Thermal characterization results

(38) Kim, Y. T.; Min, S.-K., M. *Appl. Phys. Lett.* **1991**, *59* (8), 929.
(39) Lee, C. W.; Kim, Y. T.; Min, S.-K., M. *Appl. Phys. Lett.* **1993**, *62* (25), 3312.

showed that both compounds could be effectively used as MOCVD precursors. The new compounds have been tested for the growth of tungsten nitride thin films with and without NH_3. SNMS results together with XRD data indicated that both compounds yield amorphous films of carbon-rich β-WN_xC_y and β-W_2N in the absence of NH_3. Thus, **2** and **3** behave as poor single-source precursors. When NH_3 was used as a co reactant gas during the depositions, both compounds yielded crystalline tungsten nitride films. Surprisingly, the dimethylamido compound yields a film with much less carbon contamination (2 atom %) than the hydrido compound (11 atom %) as evidenced by SNMS. This remarkable difference suggests that both compounds have quite different decomposition mechanisms even with rather than only without NH_3, which can also be seen in the TG analysis, where **2** exhibits a single-step decomposition, while the TG of **3** corresponds to a multistep decomposition process. These decomposition mechanisms are subject to current studies. Compound **2** appears to be preferable to compound **3** due to the higher growth rates as well as lower resistivity values. Optimization of several CVD parameters as well as the film thickness, morphology, resistivity, etc. is of course essential; our data presented here give just an orientation. The presence of a bulky and complex guanidinato ligand in the tungsten compounds does not necessarily have a negative influence on the precursor properties. In fact, it stabilizes the metal center and dissociates without problems. The presence of this highly tunable guanidinato ligand opens up the possibility of tailoring of many different precursors for metal nitride thin films. We suggest that the guanidinato group may play a role for metal nitride precursor development similar to that of the β-diketonates for metal oxide precursors. We intend to investigate the use of these compounds to deposit high-quality β-W_2N films using a commercial, industrial reactor of the type AIX 200 RF (Aixtron, Aachen), and currently the efforts are under way. Our results may be particularly interesting for comparison with related guanidinato-type precursors such as $[W(N\textit{i}Pr)Cl_3\{(\textit{i}PrN)_2C(NMe_2)\}]$, the synthesis and thermal properties of which McElwee-White et al. have reported recently.[33]

Acknowledgment. Financial support by the German Research Foundation (Priority Programm 1119) and the Fonds of the Chemical Industry (VCI) is gratefully acknowledged.

Supporting Information Available: X-ray crystallographic data in CIF format for the structures of compounds **1** and **3** and schemetic of the MOCVD reactor and table with film composition (PDF). This material is available free of charge via the Internet at http://pubs.acs.org.

CM061999D